



Full Length Article

Multiphoton induced photoreduction in BaFCl: Sm³⁺ nanocrystals under femtosecond laser field

Zhen Pan^a, Lianzhong Deng^{a,*}, Long Cheng^a, Yunhua Yao^a, Dalong Qi^a, Wenjing Cheng^b, Zhenrong Sun^a, Shian Zhang^{a,c,d,**}

^a State Key Laboratory of Precision Spectroscopy, School of Physics and Electronic Science, East China Normal University, Shanghai, 200241, China

^b Henan Province Engineering Research Center of Microcavity and Photoelectric Intelligent Sensing, School of Electronics and Electrical Engineering, Shangqiu Normal University, Shangqiu, 476000, China

^c Collaborative Innovation Center of Extreme Optics, Shanxi University, Taiyuan, 030006, China

^d Joint Research Center of Light Manipulation Science and Photonic Integrated Chip of East China Normal University and Shandong Normal University, East China Normal University, Shanghai, 200241, China

ARTICLE INFO

Keywords:

Photoreduction
Lanthanide-doped nanocrystals
Multiphoton excitation

ABSTRACT

Photoinduced valence state conversion in lanthanide-doped solid materials can find significant applications in areas like optical storage, opto-electronic devices and has been attracting great research efforts. Here, we experimentally demonstrate that trivalent samarium ions contained in the BaFCl nanocrystals can be efficiently reduced to divalent ones under 800 nm fs laser field. The dependences of the luminescence intensity of the photoinduced divalent ions on the femtosecond laser power, central wavelength and polarization are investigated in detail, respectively. Theoretical fits of the experimental observations indicate that a resonance-mediated (2 + 2) four-photon absorption is most probably involved in the multiphoton induced photoreduction process.

1. Introduction

Due to its potential application in high-density three-dimensional (3D) optical storage, laser induced valence state conversion in lanthanide-doped solid materials has aroused strong research interest over the past decades [1,2]. In comparison with data storage using other laser induced local modifications, such as spectral hole burning, refractive index change, nanocrystal precipitation, metal cluster or nanostructure formation, and selective spectral response of nanoparticles [3–13], the valence state conversion can offer advantages of high signal-to-noise ratio, high stability, and easy reading. Among all the materials, trivalent samarium (Sm³⁺) or europium (Eu³⁺) ion doped ones are attracting the most attention, since they can provide stable electron traps with the resulted ground state divalent ions lying below the conduction band of the host materials [14,15]. Over the years, a series of studies have been reported, exploring the influences of co-doped metal ions, charge compensation defects or laser parameters on the valence state conversion [16–19], demonstrating the prototype data storage applications [20–22], etc. Meanwhile, in search of new

lanthanide-doped materials with higher valence state conversion efficiency is also of great significance for real applications. Recent studies indicated that photoreduction in BaFCl: Sm³⁺ nanocrystals can occur with rather high efficiency under excitation of X-ray, deep UV single photon or visible multiple photons with its potential applications for multilevel optical data storage being demonstrated [23–27]. In terms of 3D optical storage application, multiphoton excitation is more favorable, since the photoinduced valence state conversion can take place only in the tightly focused laser spot where the laser intensity is strong enough to meet the multiphoton excitation threshold. And this well localized valence state conversion can offer much better spatial resolution and thus much higher optical storage density. Infrared femtosecond laser field, featuring high peak intensity and broad spectral bandwidth, has been considered as a good source for multiphoton excitation.

In this paper, infrared multiphoton induced photoreduction in BaFCl: Sm³⁺ nanocrystals, prepared by chemical coprecipitation method, is intensively studied. Under excitation of 800 nm fs laser field, highly efficient photoreduction of Sm³⁺ to Sm²⁺ has been observed to occur in the sample. The dependences of the luminescence intensity of the

* Corresponding author.

** Corresponding author. State Key Laboratory of Precision Spectroscopy, School of Physics and Electronic Science, East China Normal University, Shanghai, 200241, China.

E-mail addresses: lzdeng@phy.ecnu.edu.cn (L. Deng), sazhang@phy.ecnu.edu.cn (S. Zhang).

<https://doi.org/10.1016/j.jlumin.2023.120052>

Received 26 April 2023; Received in revised form 26 June 2023; Accepted 3 July 2023

Available online 7 July 2023

0022-2313/© 2023 Elsevier B.V. All rights reserved.

photoinduced Sm^{2+} ions on the excitation laser power, central wavelength and polarization status are investigated in detail. A multiphoton absorption model is also introduced to explain the experimental observations. And theoretical fits of the experimental results indicate that a resonance-mediated $(2 + 2)$ four-photon absorption is mainly responsible for the photoreduction process.

2. Materials and methods

The $\text{BaFCl}:\text{Sm}^{3+}$ nanoparticles were prepared by chemical coprecipitation in aqueous solution, which is similar to that of [28]. All the raw chemicals ($\text{BaCl}_2 \cdot 2\text{H}_2\text{O}$ (99.9% trace metals basis), $\text{SmCl}_3 \cdot 6\text{H}_2\text{O}$ (99.9% trace metals basis) and NH_4F (ACS reagent, $\geq 98\%$) were purchased from Sigma Company without further purification. At room temperature, 0.01 mol $\text{BaCl}_2 \cdot 2\text{H}_2\text{O}$ (99.5 mol%) and 0.05 mmol $\text{SmCl}_3 \cdot 6\text{H}_2\text{O}$ (0.5% mol%) were added in 25 mL of water and mixed under vigorous stirring. After the solution became transparent, let the resulting mixture sit for about half an hour. Then 0.01 mol of an aqueous solution of NH_4F was added to the solution under vigorous stirring. The obtained nanocrystalline precipitate was separated from the solution by centrifugation. The final product was dried at 50°C for 12 h.

The transmission electron microscopy (TEM) and X-ray diffraction (XRD) of the prepared nanoparticles are shown in Fig. 1(a) and (b), respectively. For the TEM measurement, part of the prepared sample was distributed in ethanol and ultrasonicated. The particles have an average size of less than 500 nm from analysis of the TEM image. The X-ray diffraction (XRD) of the sample was performed on a Rigaku Ultima IV X-ray diffractometer with $\text{Cu K}\alpha$ radiation ($\lambda = 1.5406$ nm), and the corresponding result is shown in Fig. 1(b) with comparison of the pattern from the standard BaFCl data (PDF#97-000-2350). All prominent peaks could be indexed to the pure tetragonal BaFCl structure with the space group of $P4/nmm$.

The schematic diagram of our experimental setup is shown in Fig. 2. Femtosecond laser pulses (central wavelength 800 nm, FWHM bandwidth ~ 30 nm, repetition rate 1 kHz) from a Ti-sapphire mode-locked regenerative amplifier (Spitfire, Spectra Physics) is used as the excitation source. The laser pulse is linearly polarized and has a time duration of about 50 fs. The laser pulse is first guided via a reflective mirror (M1) into a 4f configuration pulse shaper, which consists of two cylindrical mirrors (C1, C2), two gratings (G1, G2) and a liquid-crystal spatial light modulator (SLM-S320d, Jenoptik). Amplitude modulation of the laser pulse can be conveniently realized by programming the voltages applied on the liquid crystals of the SLM with the combination of a polarizer. The laser exiting the pulse shaper passes through a quarter wave plate ($\lambda/4$), a reflective mirror (M2), a beam splitter (BS, ratio of R/T = 50/50) and a long-wave pass dichroic mirror (DM, cutting wavelength 550 nm), and then focuses on the sample via an objective lens (OB, 10x). The fluorescence from the sample passes through the OB, the DM, the BS, a focusing lens (F1, focal length of 75 mm), a long-wave pass filter (LP, cutting wavelength 550 nm), a short-wave pass filter (SP, cutting

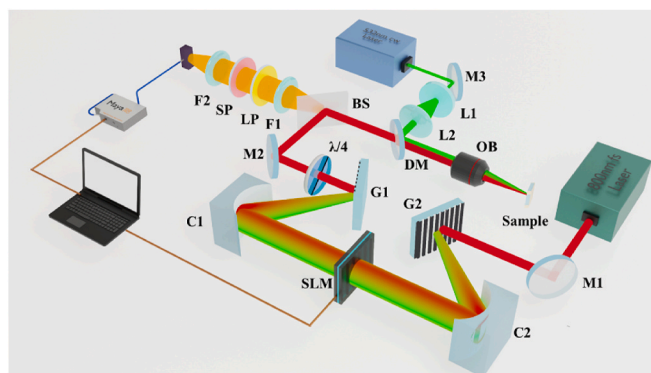


Fig. 2. Schematic diagram of the experimental setup. SLM spatial light modulator; C1, C2 cylindrical mirrors; G1, G2 gratings; M1, M2, M3 reflective mirrors; L1, L2 concave and convex lenses; DM dichroic mirror; OB objective lens; BS beam splitter; F1, F2 focusing lenses; LP long-wave pass filter; SP short-wave pass filter; $\lambda/4$ quarter wave plate.

wavelength 710 nm), a focusing lens (F2, focal length of 25 mm) and enters into a fiber spectrometer (Ocean Optics MayaPro). Signal from the fiber spectrometer is transmitted to a personal computer (PC) for post processing. A cw 532 nm laser is also used to help ascertain the presence of photoreduced samarium ions and oxidize them back to trivalent counterparts. The 532 nm laser is guided via a reflective mirror (M3) and beam shaped by a telescope (consisting of a pair of concave (L1) and convex (L2) lenses), then passes through the DM, the OB and reaches the sample.

3. Results and discussion

To confirm the occurrence of photoreduction, the luminescence spectra of the sample under 532 nm cw laser irradiation before and after 800 nm fs laser field excitation were first compared and are shown in Fig. 3(a). It is worth pointing out that excitation of the photoreduced ions (Sm^{2+}) at shorter wavelengths like 420 nm is much more efficient, however only a 532 nm laser is available for use in current study. Besides, the resolution of the spectra is instrumentally limited, since our fiber spectrometer has a spectral resolution of ~ 2.0 nm. The black solid curve (lower) shows the spectrum of the sample before femtosecond laser irradiation. There are four obvious luminescence peaks near 560, 600, 640 and 700 nm, which can be attributed to the characteristic state transitions of the Sm^{3+} ion: ${}^4\text{G}_{5/2} \rightarrow {}^6\text{H}_{5/2}$, ${}^4\text{G}_{5/2} \rightarrow {}^6\text{H}_{7/2}$, ${}^4\text{G}_{5/2} \rightarrow {}^6\text{H}_{9/2}$, ${}^4\text{G}_{5/2} \rightarrow {}^6\text{H}_{11/2}$ [29]. The red solid curve (upper) shows the corresponding spectrum after femtosecond laser excitation. In addition to the original peaks of Sm^{3+} ion, there appear new luminescence peaks at about 632, 642, 665, 688, 700 and 730 nm, which are characteristics of Sm^{2+} ion and can be assigned to state transitions of ${}^5\text{D}_1 \rightarrow 7\text{F}_J = 0,1,2$ and ${}^5\text{D}_0 \rightarrow 7\text{F}_J = 0,1,2$ [30,31]. The overlap of luminescence from both Sm^{3+}

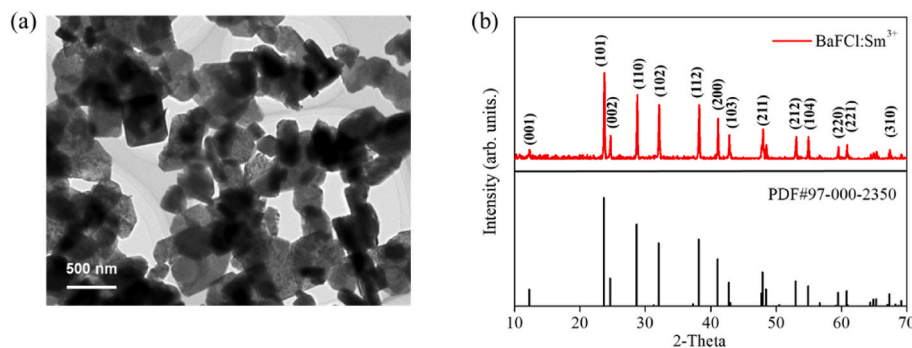


Fig. 1. (a) TEM image and (b) XRD pattern of the prepared sample.

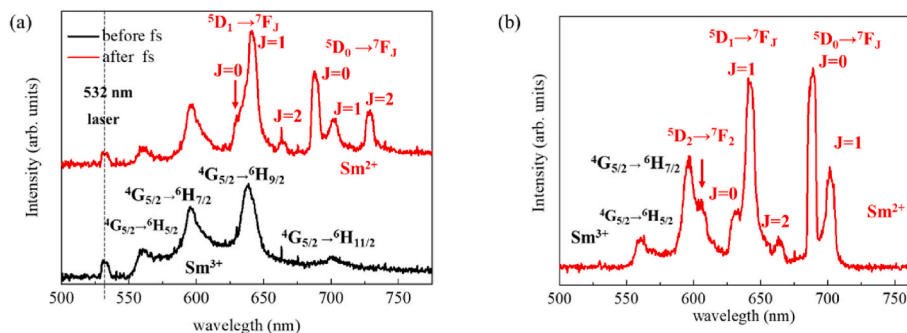


Fig. 3. (a) The luminescence spectra of the sample under 532 nm cw laser irradiation before and after 800 nm fs laser excitation. (b) The luminescence spectrum of the sample under direct 800 nm fs laser excitation.

and Sm^{2+} ions at some wavelengths is worth noting, like the peak centered at about 640 nm (Sm^{3+} : ${}^4\text{G}_{5/2} \rightarrow {}^6\text{H}_{9/2}/\text{Sm}^{2+}$: ${}^5\text{D}_1 \rightarrow {}^7\text{F}_{J=0,1,2}$). Fig. 3(b) gives the luminescence spectrum of the sample under direct femtosecond laser pulse excitation. Luminescence from both Sm^{3+} and Sm^{2+} ions can be clearly seen and is assigned appropriately. The introduction of the short-wave pass filter (cutting wavelength ~ 710 nm) for suppressing the strongly scattered signal from femtosecond laser pulse (central wavelength ~ 800 nm) cuts off the luminescence peak of Sm^{2+} ion at 730 nm (Sm^{2+} : ${}^5\text{D}_0 \rightarrow {}^7\text{F}_2$). The peaks centered at 600 nm (Sm^{3+} : ${}^4\text{G}_{5/2} \rightarrow {}^6\text{H}_{7/2}/\text{Sm}^{2+}$: ${}^5\text{D}_2 \rightarrow {}^7\text{F}_2$) and 640 nm (Sm^{3+} : ${}^4\text{G}_{5/2} \rightarrow {}^6\text{H}_{9/2}/\text{Sm}^{2+}$: ${}^5\text{D}_1 \rightarrow {}^7\text{F}_{J=0,1,2}$) contain major contributions from state transitions of both Sm^{3+} and Sm^{2+} ions. The peak centered at 688 nm is solely contributed by the Sm^{2+} ion and strong enough to serve as its indicator.

Fig. 4 shows the energy levels of the Sm^{3+} and Sm^{2+} ions together with possible state transitions involved in the processes of excitation, luminescence emission and valence state conversion. For the Sm^{3+} ion there is no real energy state for absorption of a single femtosecond laser photon (central wavelength ~ 800 nm) from the ground state ${}^6\text{H}_{5/2}$. However, non-resonant absorption of 2 fs laser photons can bring the ion to excited states of higher energy. Since the femtosecond laser has a

spectral bandwidth of ~ 30 nm, a few neighboring states of higher energy might be populated [32]. For ease of description, we just denote them as state ${}^6\text{P}_{3/2}$ here. The ions of state ${}^6\text{P}_{3/2}$ decay via phonon-assisted relaxation to state ${}^4\text{G}_{5/2}$, from which the characteristic luminescence emissions centered at about 560, 600, 640 and 700 nm are produced. Due to the ultra-high peak intensity of the femtosecond laser pulse, the Sm^{3+} ion of state ${}^6\text{P}_{3/2}$ can absorb more photons and be excited into the charge transfer band (CTB). After trapping an electron from the neighboring donor, reduction of $\text{Sm}^{3+} \rightarrow \text{Sm}^{2+}$ can occur [24]. The photoinduced Sm^{2+} ion can decay down to states like ${}^5\text{D}_2$, ${}^5\text{D}_1$, and ${}^5\text{D}_0$, from which luminescence emissions centered at about 605, 632, 642, 665, 688, 700 and 730 nm are observed. Since the temporal duration of the femtosecond laser pulse (~ 50 fs) is too short to excite the photoinduced Sm^{2+} ion for secondary luminescence. The observed luminescence in Fig. 3(b) should be from direct radiation decay of multiphoton excited Sm^{3+} ion and multiphoton induced Sm^{2+} ion.

To understand the physical mechanism for the photoreduction of $\text{Sm}^{3+} \rightarrow \text{Sm}^{2+}$ under 800 nm fs laser excitation and identify the number of photons involved in the process, we first studied the dependences of the luminescence intensities on the femtosecond laser power. Usually luminescence intensity (I) and laser power (P) have the relationship of I

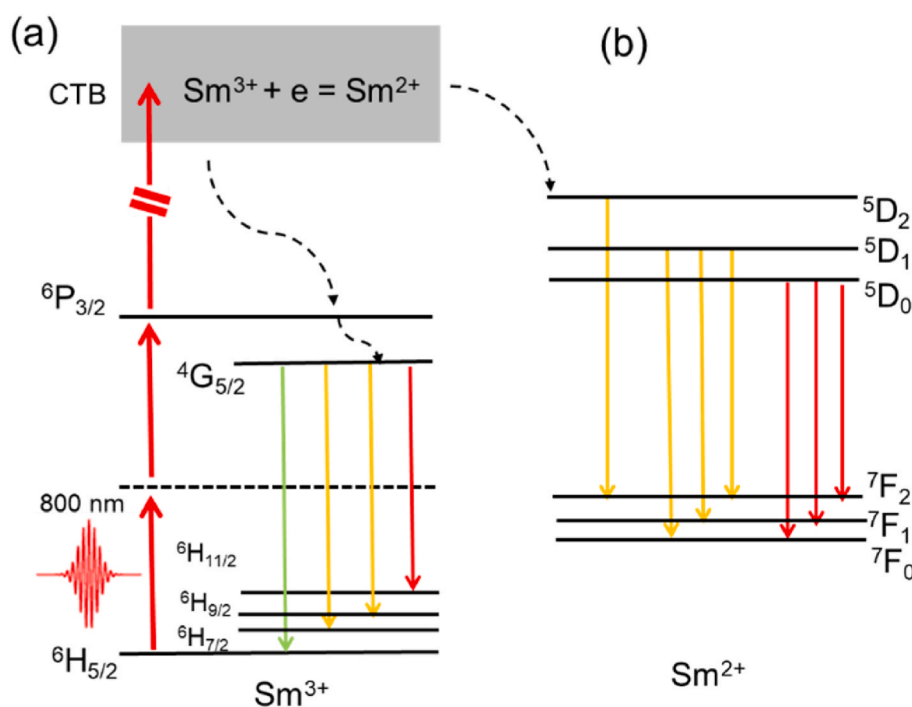


Fig. 4. Energy levels of the Sm^{3+} (a) and Sm^{2+} (b) ions together with possible state transitions involved in the processes of excitation, luminescence and valence state conversion.

$\propto P^N$, where N is the number of absorbed photons involved in the process. The integer value of N is only for ideal limit situation. In real cases, a number of factors affect the value of the slope fit and its exact value is usually smaller than the integer N [33]. The measurement was performed in such a way: The sample spot was first probed using the 532 nm cw laser (~ 30 mW) to make sure that there were no signals of Sm^{2+} ions. Then, with the help of an optical shutter 5000 fs laser pulses were allowed to hit the sample spot each time. The stable spectrum of the sample under femtosecond laser field was recorded. Before making a new measurement, the 532 nm cw laser was used again to irradiate the same sample spot. It was found in the experiment that strong luminescence signal from photoinduced Sm^{2+} ions could be observed at first but its intensity decreased dramatically upon continuous irradiation. Fig. 5 shows the spectra of the sample spot under continuous irradiation of the 532 nm cw laser at time instant of ~ 1 and ~ 60 s, respectively. As one can see, the signal of photoinduced ions can be well “erased” by the 532 nm cw laser. This kind of “erasing” signal of photoinduced ions had been observed and reported in previous studies [20,24].

The measurements were performed with the femtosecond laser power being increased from 20 to 100 mW. The area integrated signal intensities of peak 600 and 688 nm were calculated. Fig. 6 shows the corresponding results as a function of the femtosecond laser power using a log-log plot. The linear fit slopes for peak 600 (solid squares) and 688 nm (solid circles) are about 2.5 and 3.0, respectively. Since peak 688 nm is only contributed by Sm^{2+} ion, the slope of 3.0 indicates that at least three photons are involved in the photoreduction of $\text{Sm}^{3+} \rightarrow \text{Sm}^{2+}$. Peak 600 nm, however, contains contributions from both Sm^{3+} and Sm^{2+} ions, and thus has a relatively smaller slope of 2.5.

After that, the dependence of the Sm^{2+} luminescence intensity on the central wavelength of the femtosecond laser field was studied. With amplitude modulation of the pulse shaper, the femtosecond laser pulse irradiating the sample had its central wavelength shifted from 785 to 815 nm step by step. Both the step interval and the FWHM spectral bandwidth were selected to be about 5 nm. Fig. 7 shows the spectral distribution of the amplitude modulated laser pulses with the central wavelength being 785, 790, 795, 800, 805, 810 and 815 nm, respectively. The average power of the femtosecond laser pulses was fixed at about 30 mW. Similarly, for each new measurement, the sample spot was first irradiated by the 532 nm cw laser to “erase” the Sm^{2+} ions. The luminescence spectra of the sample under the above shaped

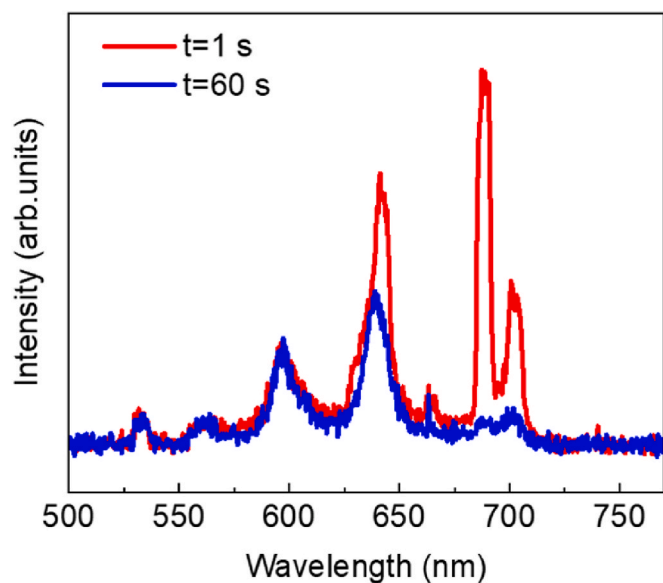


Fig. 5. Spectra of the sample spot under continuous “erasing” of the 532 nm cw laser (~ 30 mW) at time instant of ~ 1 and ~ 60 s, respectively. The sample spot was first excited by 5000 fs laser pulses.

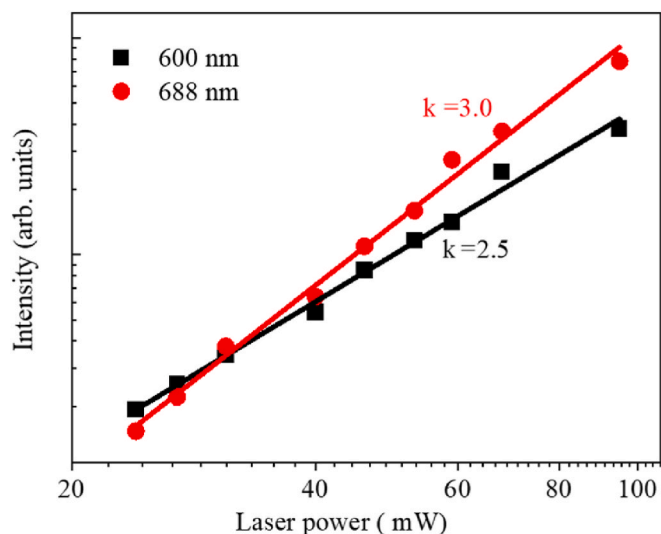


Fig. 6. The laser power dependences of peak 600 and 688 nm intensities under 800 nm fs laser field excitation.

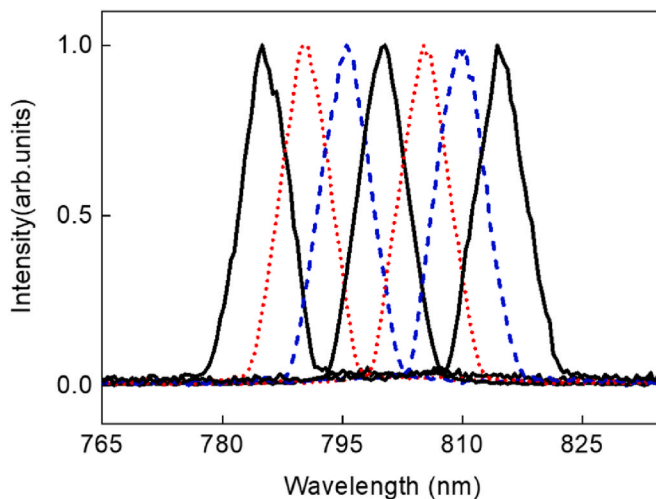


Fig. 7. The spectral distribution of the amplitude modulated laser pulses with the central wavelength being 785, 790, 795, 800, 805, 810 and 815 nm (from left to right), respectively.

femtosecond laser pulses were recorded and plotted in Fig. 8(a). The area integrated signal intensity of peak 688 nm was calculated and presented in Fig. 8(b) (solid squares). The solid line is a Lorentz fit of the experimental data with the peak center appearing at about 802 nm. As the laser central wavelength is tuned away from 802 nm, the signal intensity of peak 688 nm decreases dramatically. This central laser wavelength dependence of the Sm^{2+} luminescence intensity can be explained as follows: when the laser central wavelength is tuned at about 802 nm, the non-resonant two-photon absorption is centered at about 401 nm, and the intermediate state ${}^6P_{3/2}$ of the sample can be most effectively populated with the corresponding photoreduction effect being the best.

For further exploring the underlying mechanism of the photoreduction, a $\lambda/4$ wave plate was used to change the polarization state of the femtosecond laser pulse, and the dependence of the photoreduction on the laser polarization was studied. While keeping the output laser power constant, the polarization state can be changed by varying the angle θ between the linear polarization direction of the input laser and the optical axis of the $\lambda/4$ wave plate. The polarization of the laser field is linear for $\theta = m\pi/2$ ($m = 0, 1, 2 \dots$), circular for $\theta = (2m + 1)\pi/4$ ($m =$

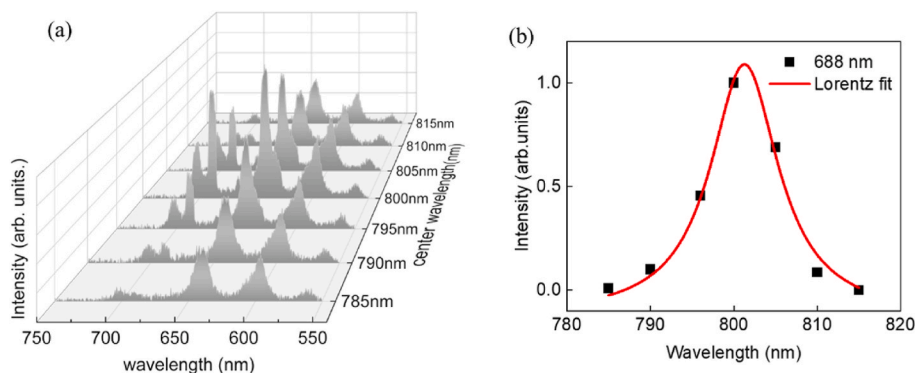


Fig. 8. (a) Luminescence spectra of the sample and (b) corresponding signal intensities of peak 688 nm under direct femtosecond laser field with central wavelength being 785, 790, 795, 800, 805, 810 and 815 nm, respectively.

0, 1, 2 ...) and elliptical for θ of other angles.

The luminescence spectra of the sample under 800 nm fs laser field of various polarization state were recorded. Similarly, for each new measurement the sample spot was first “erased” by the 532 nm cw laser. Fig. 9 shows the luminescence spectra with the angle θ changing from 0° to 180° . As one can see, the heights of the luminescence peaks vary dramatically with changing θ . The area integrated signals of the peaks centered at 600 and 688 nm are calculated and presented in Fig. 10(a) and (b) (solid squares), respectively. Periodic variation of the peak signals with changing θ can be clearly seen. For $\theta = 0^\circ, 90^\circ$ and 180° , the output laser is linearly polarized and the maximal peak intensities are obtained; For $\theta = 45^\circ$ and 135° , the output laser is circularly polarized and the minimal peak intensities are obtained; For other θ values, the output laser is elliptically polarized and the peak intensities are in between. The ratio of the minimal signal value to the maximal signal value, defined as polarization modulation depth here, is about ~ 0.34 and ~ 0.25 for the peak 600 and 688 nm, respectively. The black dotted line, red solid line and blue solid line are theoretical fits from the expressions of $I_1 = [\cos^4(\theta) + \sin^4(\theta)]$, $I_2 = [\cos^4(\theta) + \sin^4(\theta)] \times [\cos^4(\theta) + \sin^4(\theta)]$ and $I_3 = [0.3 * I_1 + 0.7 * I_2]$, respectively. As one can see, the experimental data for peak 688 and 600 nm can be well fitted by the expressions of I_2 and I_3 , respectively.

To further understand the polarization dependences of the $\text{Sm}^{3+}/\text{Sm}^{2+}$ luminescence intensities under femtosecond laser field and ascertain the number of photons involved in the process, let us turn to

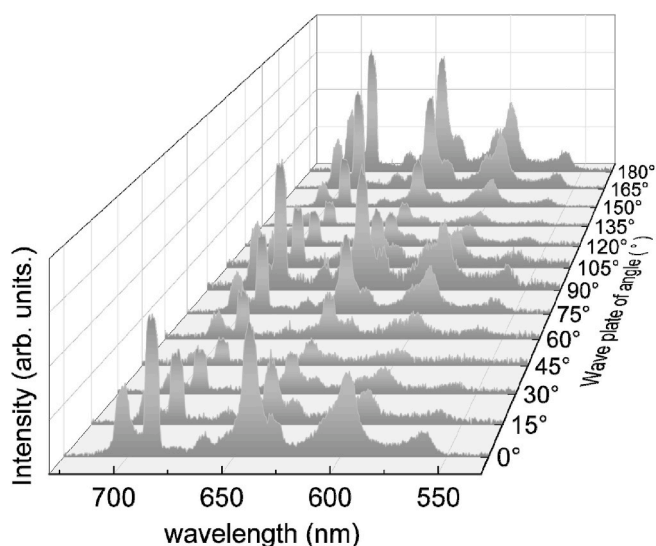


Fig. 9. Spectra of the sample under 800 nm fs laser field of various polarization state.

the theoretical model of multiphoton absorption. Fig. 11 shows a schematic diagram of the resonance-mediated ($n + m$) multiphoton absorption process in the ion system excited by the femtosecond laser pulse $E(t)$, where $|g\rangle$, $|i\rangle$ and $|f\rangle$ represent the ground state, the intermediate state and the final state, respectively. Ion of state $|g\rangle$ is first excited to state $|i\rangle$ by absorbing n photons and then further excited to state $|f\rangle$ by absorbing m more photons simultaneously. When the intermediate state $|i\rangle$ is real, the transition probability from state $|g\rangle$ to state $|f\rangle$ will be greatly improved, corresponding to the so-called resonance mediated ($n + m$) multiphoton absorption. In theory, the multiphoton absorption in the broadband absorption system can be considered as a sum of each individual transition. On the basis of the theoretical model of the atomic system with a narrow absorption line limit [34,35], the transition probabilities to states $|i\rangle$ and $|f\rangle$, denoted as A_i and A_f , can be approximated in the frequency domain as

$$A_i = \frac{1}{\hbar^{2n}} \int_{-\infty}^{+\infty} D(\omega_i) \left| \int_{-\infty}^{+\infty} \mu_{g \rightarrow i} \vec{E}(t) \times \exp(i\omega_i t) dt \right|^2 d\omega_i \quad (1)$$

$$A_f = \frac{1}{\hbar^{2(n+m)}} \int_{-\infty}^{+\infty} D(\omega_f) \left| \int_{-\infty}^{+\infty} D(\omega_i) \mu_{g \rightarrow i} \mu_{i \rightarrow f} \times \int_{-\infty}^{+\infty} E^{\rightarrow n}(t_1) E^{\rightarrow m}(t_2) \exp[i(\omega_f - \omega_i)t_1] \times \exp(i\omega_i t_2) dt_2 dt_1 d\omega_i \right|^2 d\omega_f \quad (2)$$

Here \hbar is the Planck constant, $D(\omega_i)$ and $D(\omega_f)$ are the ion absorption line-shape function in the $|i\rangle$ state and $|f\rangle$ state, $\mu_{g \rightarrow i}$ and $\mu_{i \rightarrow f}$ are the effective dipole coupling for the state transitions $|g\rangle \rightarrow |i\rangle$ and $|i\rangle \rightarrow |f\rangle$; ω_i and ω_f are the frequencies for the state transitions $|g\rangle \rightarrow |i\rangle$ and $|g\rangle \rightarrow |f\rangle$.

When a linearly polarized laser field, $\vec{E}(t) = E_0(t)\cos(\omega t)\vec{e}_x$, is incident into a quarter wave plate ($\lambda/4$ wave plate), the output laser field can be written as

$$\vec{E}'_q(t) = E_0(t) \left[\cos(\theta)\cos(\omega t)\vec{e}_x + \sin(\theta)\cos(\omega t + \pi/2)\vec{e}_y \right] \quad (3)$$

With θ being the angle between the polarization direction of the input laser field and the optical axis of the $\lambda/4$ wave plate. For the resonance-mediated ($n + m$) multiphoton absorption process, all the n (or m) photons involved in the nonresonant absorption should have the same polarization direction, but their polarization direction may be different from that of the m (or n) photons. Thus, A_i and A_f of equations (1) and (2) can be further written as

$$A_i = [\cos^{2n}(\theta) + \sin^{2n}(\theta)] \frac{1}{\hbar^{2n}} \int_{-\infty}^{+\infty} D(\omega_i)$$

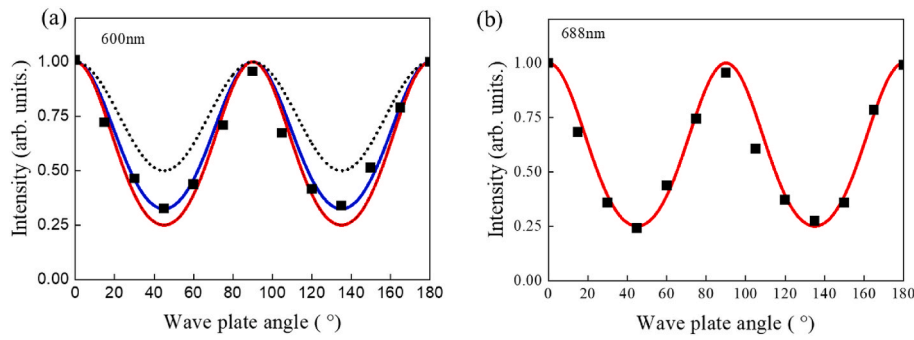


Fig. 10. The laser polarization dependences of peak 600 (a) and 688 nm (b) intensities under 800 nm fs laser field, respectively.

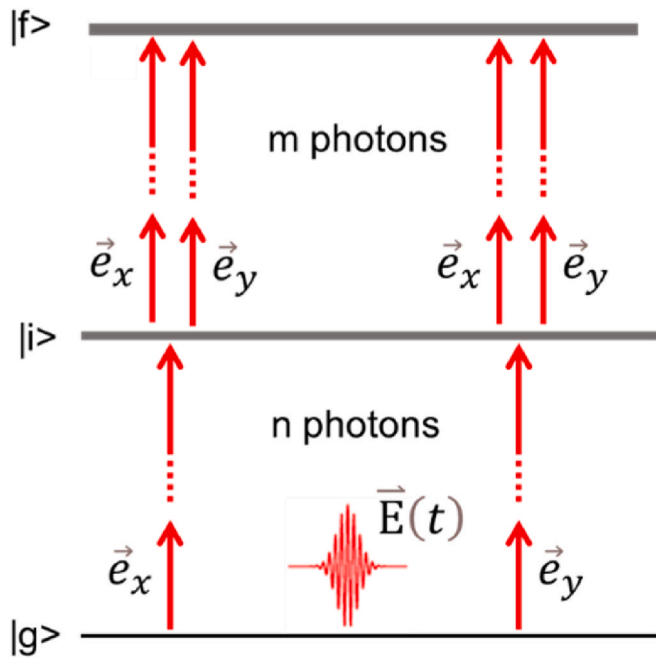


Fig. 11. Schematic diagram of the resonance-mediated $(n + m)$ multiphoton absorption model.

$$\times \left| \int_{-\infty}^{+\infty} \mu_{g \rightarrow i} \vec{E}^n(t) \exp(i\omega_i t) dt \right|^2 d\omega_i \quad (4)$$

$$A_f = \{ [\cos^{2n}(\theta) + \sin^{2n}(\theta)] \times [\cos^{2m}(\theta) + \sin^{2m}(\theta)] \}$$

$$\times \frac{1}{\hbar^{2(n+m)}} \int_{-\infty}^{+\infty} D(\omega_f) \times \left| \int_{-\infty}^{+\infty} \mu_{g \rightarrow i} \mu_{i \rightarrow j} D(\omega_i) \right.$$

$$\times \int_{-\infty}^{+\infty} \int_{-\infty}^{t_1} \vec{E}^n(t_1) \vec{E}^m(t_2) \exp[i(\omega_f - \omega_i)t_1] \times \exp(i\omega_i t_2) dt_2 dt_1 d\omega_i \left. \right|^2 d\omega_f \quad (5)$$

As can be seen from above equations, both A_i and A_f have a strong dependence on the laser polarization. A_i is proportional to the value of expression $[\cos^{2n}(\theta) + \sin^{2n}(\theta)]$ and A_f is proportional to the value of expression $[\cos^{2n}(\theta) + \sin^{2n}(\theta)] \times [\cos^{2m}(\theta) + \sin^{2m}(\theta)]$. When $\theta = m\pi/2$ ($m = 0, 1, 2 \dots$), the maximal value of unity is obtained for both expressions; when $\theta = m\pi/4$ ($m = 0, 1, 2 \dots$) the minimal value is obtained for both expressions. For the case of photoreduction of $\text{Sm}^{3+} \rightarrow \text{Sm}^{2+}$

under 800 nm fs laser field here, the above states $|g\rangle$, $|i\rangle$ and $|f\rangle$ correspond to the real energy states ${}^6\text{H}_{5/2}$, ${}^6\text{P}_{3/2}$ and CTB of the Sm^{3+} ion, respectively. Since state ${}^6\text{P}_{3/2}$ can be approached by two photons, the value of n is 2. The signal intensity of peak 688 nm, an indicator of photoinduced Sm^{2+} ions, is proportional to the value of A_f . As shown in Fig. 10(b), the experimental data for its laser polarization dependence is well fitted using the expression $[\cos^{2n}(\theta) + \sin^{2n}(\theta)] \times [\cos^{2m}(\theta) + \sin^{2m}(\theta)]$ with $n = 2$ and $m = 2$, and the corresponding polarization modulation depth is 0.25 in theory, rather close to the experimental value of ~ 0.25 . This indicates that a resonance-mediated $(2 + 2)$ four-photon absorption process should be mainly involved in the photoreduction of $\text{Sm}^{3+} \rightarrow \text{Sm}^{2+}$ here. One thing worth pointing is that a resonance-mediated $(2 + 1)$ three-photon absorption process might contribute somewhat to the photoreduction. However, with $n = 2$ and $m = 1$ the corresponding polarization modulation depth is only 0.5 in theory, which is far from the observed value of ~ 0.25 . Therefore, even if there exists some kind of resonance-mediated $(2 + 1)$ three-photon absorption, its contribution to the photoreduction of $\text{Sm}^{3+} \rightarrow \text{Sm}^{2+}$ should be rather small. The signal peak of 600 nm, however, contains luminescence contributions from both Sm^{2+} and Sm^{3+} ions. As discussed above, the luminescence contribution of Sm^{2+} has a polarization modulation depth of 0.25 in theory. The luminescence contribution of Sm^{3+} , however, can come from two channels. One channel is: ${}^6\text{H}_{5/2}$ (non-resonant two-photon absorption) \rightarrow ${}^6\text{P}_{3/2}$ (phonon-assisted relaxation) \rightarrow ${}^4\text{G}_{5/2}$ (luminescence) \rightarrow ${}^6\text{H}_{7/2}$. The luminescence involves non-resonant two-photon absorption and has a polarization modulation depth of 0.5 in theory. Another channel is: ${}^6\text{H}_{5/2}$ (non-resonant two-photon absorption) \rightarrow ${}^6\text{P}_{3/2}$ (non-resonant two-photon absorption) \rightarrow CTB (phonon-assisted relaxation back to) \rightarrow ${}^4\text{G}_{5/2}$ (luminescence) \rightarrow ${}^6\text{H}_{7/2}$. Since not all the Sm^{3+} ions excited into the CTB can succeed in trapping an electron and being photoreduced to Sm^{2+} , some of them can decay back via phonon-assisted relaxation to low-lying ${}^4\text{G}_{5/2}$ states and emit luminescence. The corresponding luminescence involves resonance-mediated $(2 + 2)$ four-photon absorption and share the same polarization modulation depth of 0.25 as that from Sm^{2+} in theory. And this explains the observed polarization modulation depth of ~ 0.34 for the signal peak of 600 nm.

4. Conclusion

In summary, we have studied the photoreduction in BaFCl: Sm^{3+} nanocrystals under 800 nm fs laser field. Highly efficient photoreduction of $\text{Sm}^{3+} \rightarrow \text{Sm}^{2+}$ can occur under infrared multiphoton excitation. For deep understanding the mechanism behind the photoreduction process, the dependences of the luminescence intensity of the photoinduced divalent ions on the excitation laser power, central wavelength and polarization were carefully investigated. Experimental results indicate that the photoreduction process has a strong dependence on the central wavelength of the femtosecond laser and confirm the direct involvement of the intermediate ${}^6\text{P}_{3/2}$ state of the Sm^{3+} ion. A resonance-mediated multi-photon absorption theoretical model was introduced to help explain the laser polarization dependences of the $\text{Sm}^{3+}/\text{Sm}^{2+}$

luminescence intensities. Theoretical fits of the experimental data indicate that the resonance-mediated (2 + 2) four-photon absorption should be the most probable channel exciting the ground state Sm^{3+} into the charge transfer band, leading to the photoreduction of $\text{Sm}^{3+} \rightarrow \text{Sm}^{2+}$. Our studies show that BaFCl: Sm^{3+} nanocrystals under infrared multiphoton excitation can be a good potential candidate for 3D optical data storage. Besides, compared to UV single photon excitation, infrared multiphoton excitation can bring much higher spatial resolution, particularly in the direction of laser propagation, which is of great significance for practical 3D optical storage of ultrahigh density.

Author contributions

Conceptualization, L. Deng, S. Zhang; material preparation, Z. Pan; data acquisition, Z. Pan, L. Cheng; data analysis, Z. Pan, L. Deng; writing - original draft, Z. Pan, L. Deng, review and editing, L. Deng, Y. Yao, D. Qi, W. Cheng, Z. Sun, S. Zhang; funding acquisition, L. Deng, Y. Yao, D. Qi, W. Cheng, Z. Sun, S. Zhang.

Declaration of competing interest

The authors declare that they have no known competing financial interests or personal relationships that could have appeared to influence the work reported in this paper.

Data availability

Data will be made available on request.

Acknowledgements

The authors acknowledge funding from the National Natural Science Foundation of China (62175066, 62105101, 92150301, 12074121, 12034008, 12274129, 12274139, 12004238) and the Science and Technology Commission of Shanghai Municipality (21XD1400900, 20ZR1417100, 21JM0010700).

References

- [1] J. Qiu, K. Miura, T. Suzuki, T. Mitsuyu, K. Hirao, Permanent photoreduction of Sm^{3+} to Sm^{2+} inside a sodium aluminoborate glass by an infrared femtosecond pulsed laser, *Appl. Phys. Lett.* 74 (1999) 10–12.
- [2] K. Miura, J. Qiu, S. Fujiwara, S. Sakaguchi, K. Hirao, Three-dimensional optical memory with rewriteable and ultrahigh density using the valence-state change of samarium ions, *Appl. Phys. Lett.* 80 (2002) 2263–2265.
- [3] R. Jaaniso, H. Bill, Room temperature persistent spectral hole burning in Sm-doped $\text{SrF}_{11/2}\text{Br}_{1/2}$ mixed crystals, *Europhys. Lett.* 16 (1991) 569–574.
- [4] M. Nogami, Y. Abe, K. Hirao, D.H. Cho, Room temperature persistent spectra hole burning in Sm^{2+} -doped silicate glasses prepared by the sol-gel process, *Appl. Phys. Lett.* 66 (1995) 2952–2954.
- [5] E.N. Glezer, M. Milosavljevic, L. Huang, R.J. Finlay, T.-H. Her, J.P. Callan, E. Mazur, Three-dimensional optical storage inside transparent materials, *Opt. Lett.* 21 (1996) 2023–2025.
- [6] D. Tan, X. Sun, Q. Wang, P. Zhou, Y. Liao, J. Qiu, Fabricating low loss waveguides over a large depth in glass by temperature gradient assisted femtosecond laser writing, *Opt. Lett.* 45 (2020) 3941–3944.
- [7] J. Qiu, X. Jiang, C. Zhu, M. Shirai, J. Si, N. Jiang, K. Hirao, Manipulation of gold nanoparticles inside transparent materials, *Angew. Chem., Int. Ed.* 43 (2004) 2230–2234.
- [8] X. Huang, Q. Guo, D. Yang, X. Xiao, X. Liu, Z. Xia, F. Fan, J. Qiu, G. Dong, Reversible 3D laser printing of perovskite quantum dots inside a transparent medium, *Nat. Photonics* 14 (2019) 82–88.
- [9] A. Royon, K. Bourhis, M. Bellec, G. Papon, B. Bousquet, Y. Deshayes, T. Cardinal, L. Canioni, Silver clusters embedded in glass as a perennial high capacity optical recording medium, *Adv. Mater.* 22 (2010) 5282–5286.
- [10] J. Zhang, M. Gecevicius, M. Beresna, P.G. Kazansky, Seemingly unlimited lifetime data storage in nanostructured glass, *Phys. Rev. Lett.* 112 (2014), 033901.
- [11] Y. Shimotsuna, M. Sakakura, P.G. Kazansky, M. Beresna, J. Qiu, K. Miura, K. Hirao, Ultrafast manipulation of self-assembled form birefringence in glass, *Adv. Mater.* 22 (2010) 4039–4043.
- [12] H. Dittlacher, J.R. Krenn, B.L. Amprecht, A. Leitner, F.R. Aussenegg, Spectrally coded optical data storage by metal nanoparticles, *Opt. Lett.* 25 (2000) 563–565.
- [13] P. Zijlstra, J.W. Chon, M. Gu, Five-dimensional optical recording mediated by surface plasmons in gold nanorods, *Nature* 459 (2009) 410–413.
- [14] P. Dorenbos, Systematic behaviour in trivalent lanthanide charge transfer energies, *J. Phys. Condens. Matter* 15 (2003) 8417.
- [15] P. Dorenbos, Valence stability of lanthanide ions in inorganic compounds, *Chem. Mater.* 17 (2005) 6452–6456.
- [16] M. Nogami, G. Kawamura, G.J. Park, H. You, T. Hayakawa, Effect of Al^{3+} and Ti^{4+} ions on the laser reduction of Sm^{3+} ion in glass, *J. Lumin.* 114 (2005) 178–186.
- [17] S. Park, Y. Chung, W. Qin, H. Cho, E. Cho, K. Jang, S. Kim, Y.-I. Lee, C. Kim, The influence of metal aluminium on the reduction of the Sm^{3+} doped in aluminosilicate glass films, *J. Phys. Condens. Matter* 16 (2004) 2543–2549.
- [18] M. Tsuta, S. Nakamura, A. Kato, Effect of laser fluence and charge compensation defects on photoreduction of Eu ions in KSRPO_4 crystal using a UV laser, *J. Lumin.* 244 (2022), 118755.
- [19] Y. Zheng, Y. Yao, L. Deng, W. Cheng, J. Li, T. Jia, J. Qiu, Z. Sun, S. Zhang, Valence state manipulation of Sm^{3+} ions via a phase-shaped femtosecond laser field, *Photon. Res.* 6 (2018) 144–148.
- [20] K. Miura, J. Qiu, S. Fujiwara, S. Sakaguchi, K. Hirao, Three-dimensional optical memory with rewriteable and ultrahigh density using the valence-state change of samarium ions, *Appl. Phys. Lett.* 80 (2002) 2263–2265.
- [21] J. Lim, M. Lee, E. Kim, Three-dimensional optical memory using photoluminescence change in Sm-doped sodium borate glass, *Appl. Phys. Lett.* 86 (2005), 191105.
- [22] Z. Wang, D. Tan, J. Qiu, Single-shot photon recording for three-dimensional memory with prospects of high capacity, *Opt. Lett.* 45 (2020) 6274–6277.
- [23] N. Riesen, A. Francois, K. Badek, T.M. Monro, H. Riesen, Photoreduction of Sm^{3+} in nanocrystalline BaFCl, *J. Phys. Chem.* 119 (2015) 6252–6256.
- [24] H. Riesen, K. Badek, T.M. Monro, N. Riesen, Highly efficient valence state switching of samarium in BaFCl: Sm nanocrystals in the deep UV for multilevel optical data storage, *Opt. Mater. Express* 6 (2016) 3097–3108.
- [25] N. Riesen, X. Pan, K. Badek, Y. Ruan, T.M. Monro, J. Zhao, H.E. Heidepriem, H. Riesen, Towards rewritable multilevel optical data storage in single nanocrystals, *Opt Express* 26 (2018) 12266–12275.
- [26] N. Riesen, C. Priest, D.G. Lancaster, K. Badek, H. Riesen, Ultra-high-resolution greyscale fluorescence images via UV-exposure of thin flexible phosphor films, *Nanoscale* 15 (2023) 4863–4869.
- [27] N. Riesen, K. Badek, H. Riesen, Data storage in a nanocrystalline mixture using room temperature frequency-selective and multilevel spectral hole-burning, *ACS Photonics* 8 (2021) 3078–3084.
- [28] H. Riesen, W.A. Kaczmarek, Efficient x-ray generation of Sm^{2+} in nanocrystalline BaFCl/ Sm^{3+} : a photoluminescent x-ray storage phosphor, *Inorg. Chem.* 46 (2007) 7235–7237.
- [29] J. Li, L. Deng, Y. Zheng, P. Ding, T. Jia, Z. Sun, J. Qiu, S. Zhang, Optimal spectral phase control of femtosecond laser-induced up-conversion luminescence in Sm^{3+} : NaYF₄ glass, *Front. Physiol.* 15 (2020), 22601.
- [30] Q. Zeng, N. Kilah, M. Riley, H. Riesen, Luminescence properties of Sm^{2+} -activated barium chloroborates, *J. Lumin.* 104 (2003) 65–76.
- [31] Y. Huang, W. Kai, Y. Cao, K. Jang, H.S. Lee, I. Kim, E. Cho, Spectroscopic and structural studies of Sm^{2+} doped orthophosphate KSRPO_4 crystal, *J. Appl. Phys.* 103 (2008), 053501.
- [32] W.T. Carnall, P.R. Fields, K. Rajnak, Electronic energy levels in the trivalent lanthanide aquo ions. I. Pr^{3+} , Nd^{3+} , Pm^{3+} , Sm^{3+} , Dy^{3+} , Ho^{3+} , Er^{3+} , and Tm^{3+} , *J. Chem. Phys.* 49 (1968) 4424–4442.
- [33] M. Pollnau, D.R. Gamelin, S.R. Lüthi, H.U. Güdel, M.P. Hehlen, Power dependence of upconversion luminescence in lanthanide and transition-metal-ion systems, *Phys. Rev. B* 61 (2000) 3337–3346.
- [34] D. Meshulach, Y. Silberberg, Coherent quantum control of multiphoton transitions by shaped ultrashort optical pulses, *Phys. Rev. Appl.* 60 (1999) 1287–1292.
- [35] A. Gandman, L. Chuntanov, L. Rybak, Z. Amitay, Coherent phase control of resonance-mediated (2+1) three-photon absorption, *Phys. Rev. Appl.* 75 (2007), 031401.